THE JOURNAL OF BIOLOGICAL CHEMISTRY VOL. 289, NO. 35, pp. 24180–24187, August 29, 2014

Binding of TPP1 Protein to TIN2 Protein Is Required for POT1a,b Protein-mediated Telomere Protection*

Received for publication, June 30, 2014, and in revised form, July 22, 2014 Published, JBC Papers in Press, July 23, 2014, DOI 10.1074/jbc.M114.592592

David Frescas and Titia de Lange[1]

From the Laboratory for Cell Biology and Genetics, The Rockefeller University, New York, New York 10065

Background: Chromosome ends require the TPP1/POT1 heterodimers for protection.
Results: A TIN2 mutant that fails to bind TPP1 resulted in phenotypes associated with TPP1/POT1 deletion.
Conclusion: The TIN2-TPP1 link is the sole mechanism by which TPP1/POT1 heterodimers bind to shelterin to protect telomeres.
Significance: The function of TIN2 is relevant to dyskeratosis congenita cases caused by TIN2 mutations.

The single-stranded DNA binding proteins in mouse shelterin, POT1a and POT1b, accumulate at telomeres as heterodimers with TPP1, which binds TIN2 and thus links the TPP1/POT1 dimers with TRF1 and TRF2/Rap1. When TPP1 is tethered to TIN2/TRF1/TRF2, POT1a is thought to block replication protein A binding to the single-stranded telomeric DNA and prevent ataxia telangiectasia and Rad3-related kinase activation. Similarly, TPP1/POT1b tethered to TIN2 can control the formation of the correct single-stranded telomeric overhang. Consistent with this view, the telomeric phenotypes following deletion of POT1a,b or TPP1 are phenocopied in TIN2-deficient cells. However, the loading of TRF1 and TRF2/Rap1 is additionally compromised in TIN2 KO cells, leading to added phenotypes. Therefore, it could not be excluded that, in addition to TIN2, other components of shelterin contribute to the recruitment of TPP1/POT1a,b as suggested by previous reports. To test whether TIN2 is the sole link between TPP1/POT1a,b and telomeres, we defined the TPP1 interaction domain of TIN2 and generated a TIN2 allele that was unable to interact with TPP1 but retained its interaction with TRF1 and TRF2. We demonstrated that cells expressing TIN2ΔTPP1 instead of wild-type TIN2 phenocopy the POT1a,b knockout setting without showing additional phenotypes. Therefore, these results are consistent with TIN2 being the only mechanism by which TPP1/POT1 heterodimers bind to shelterin and function in telomere protection.

Shelterin, a telomere-specific protein complex, represses DNA damage signaling by the ataxia telangiectasia mutated (ATM)[2] and ataxia telangiectasia and Rad3-related (ATR) kinases and prevents double strand break repair at chromosome ends (1). The conditional deletion of individual shelterin proteins has revealed substantial functional compartmentalization within shelterin. For example, TRF2 is required for the repression of ATM-dependent signaling and classical non-homologous end joining, whereas the closely related TRF1 protein prevents replication fork stalling in telomeric DNA and represses the accompanying telomere fragility. POT1a prevents ATR kinase signaling at telomeres by blocking the binding of RPA to the single-stranded TTAGGG repeats, whereas POT1b is required for the correct formation of the 3′ telomeric overhang after telomere replication.

Essential to the function of POT1 is the formation of a heterodimeric complex with TPP1 and the binding of these TPP1/POT1 heterodimers to TIN2, the central component of shelterin (2–4). TIN2 interacts with TRF1 and TRF2 to associate with telomeres (2–4). Consistent with the role of TIN2 as the bridge that links TPP1/POT1 to shelterin, deletion of TIN2 phenocopies the loss of TPP1 and/or POT1a,b, including the activation of ATR signaling, excessive single-stranded telomeric DNA, and occasional telomere fusions (5–8).

However, complicating the analysis of TIN2 in facilitating TPP1/POT1 function within shelterin is the activation of ATM kinase signaling and a moderate level of chromosome-type telomere fusions following TIN2 deletion, each of which are hallmarks of TRF2 loss (8–10). Although the chromosome-type fusions following TIN2 deletion are due to decreased telomeric accumulation of TRF2, the ATM kinase signaling observed in TIN2 KO cells, which remains despite forced expression of exogenous TRF2, suggests that TIN2 plays a direct role in the repression of ATM by TRF2 (5). In addition to diminishing the loading of TRF2, TIN2 deficiency results in the reduced presence of TRF1 on telomeres and decreased TRF1 protein levels, although the amount of TRF1 appears to be sufficient to prevent overt TRF1 deficiency phenotypes. Finally, several reports have proposed an interaction between TRF2 and POT1 in human cells (3, 11, 12), raising the possibility that the POT1a,b DKO (double knockout) phenotypes associated with TIN2 deletion may be a consequence of both the lack of the TIN2-TPP1 tether and the loss of TRF2 from telomeres.

Studying the role of TIN2 in shelterin is particularly important because a number of TIN2 mutations have been identified

* This work was supported, in whole or in part, by National Institutes of Health Grants 5R37GM49046 and 5RO1AG16642 (to D. F.). This work was also supported by an American Cancer Society postdoctoral fellowship (to D. F.).
[1] American Cancer Society Research Professor. To whom correspondence should be addressed: Box 159, The Rockefeller University, 1230 York Ave., New York, NY 10065. Tel.: 212-327-8146; Fax: 212-327-7147; E-mail: delange@mail.rockefeller.edu.
[2] The abbreviations used are: ATM, ataxia telangiectasia mutated; ATR, ataxia telangiectasia and Rad3-related; DC, dyskeratosis congenita; MEF, mouse embryonic fibroblast; ATRi, ataxia telangiectasia and Rad3-related inhibitor; TIF, telomere dysfunction-induced focus/foci; IF, immunofluorescence; EV, empty vector.

in dyskeratosis congenita (DC), a rare inherited bone marrow failure syndrome belonging to a group of telomeropathies caused by defective telomere maintenance (13–17). The unifying feature present in DC patients is abnormally short telomeres, and patients harboring TIN2 mutations possess extremely short telomeres and have an increased severity of the disease. Importantly, in addition to accelerated telomere shortening, mouse embryonic fibroblasts (MEFs) isolated from mice expressing a knockin TIN2 DC allele showed ATR signaling at telomeres and an increased frequency of signal-free chromosome ends and fragile telomeres (18), suggesting a complex telomere maintenance and protection defect. Because the exact basis of these defects has not been determined, additional functional studies of TIN2 are crucial to understanding the diverse roles TIN2 plays within shelterin.

Because of the confounding effects of TIN2 deletion on TRF2/Rap1 and TRF1, it is difficult to determine whether the loss of TPP1/POT1 function in the TIN2 KO cells is solely due to the absence of TIN2 or is, in part, due to the absence of (redundant) interactions with other shelterin components. Therefore, we generated an allele of TIN2 that fails to bind TPP1 but is proficient in maintaining its interactions with TRF1 and TRF2 and supports their normal accumulation at telomeres. We show that severing the TIN2-TPP1 interaction faithfully recapitulates the phenotypes observed in TPP1 KO and POT1a,b DKO cells without affecting TRF1 or TRF2, therefore providing direct evidence that TPP1/POT1a,b requires its connection to the shelterin complex via TIN2 to protect telomeres.

EXPERIMENTAL PROCEDURES

Cell lines and Expression Plasmids—SV40-LT-immortalized $TIN2^{F/F}$ cells (5) were grown in DMEM supplemented with L-glutamine, penicillin/streptomycin, nonessential amino acids, and 10% fetal bovine serum (Invitrogen). 293T cells were maintained in DMEM supplemented with L-glutamine, penicillin/streptomycin, nonessential amino acids, and 10% bovine calf serum (BCS) (Hyclone). $TIN2^{F/F}$ MEFs were infected with pWZL-hygromycin retroviruses expressing FLAG-HA-HA (FLAG-HA2)-tagged mouse TIN2 alleles or an empty vector and selected with hygromycin as described previously (19). In some experiments, the hygromycin-selected MEFs were subsequently infected with pLPC-puromycin retroviruses expressing MYC-tagged TPP1 (6) or POT1b (7). In all cases, following three rounds of retroviral infection, MEFs were selected with hygromycin or puromycin, respectively, for 2–4 days. For immunoprecipitation studies, 293T cells were transiently cotransfected with MYC-tagged TRF2 or TPP1 plasmids (pLPC-based) and FLAG-HA2-tagged mouse TIN2 alleles (pLPC-based) using the calcium phosphate coprecipitation method. The introduced deletion in TIN2 was made using a QuikChange II site-directed mutagenesis kit (Agilent Technologies) and confirmed by DNA sequencing. N-terminal TIN2 truncation alleles were generated by PCR and introduced into the FLAG-pLPC vector. The ExPASy Proteomics Tools Server was used to predict secondary structure. Deletion of floxed alleles in all MEF lines was induced by two infections with the Hit&Run Cre retrovirus at 12-hour intervals as described previously (19). Time points were defined in hours or days after the second infection. The ATR inhibitor (ATRi) was ETP46464 (20) used at 1.0 μM. The ATM inhibitor and ATRi were added to tissue culture medium 24 h after the Cre infection and 48 h before the analysis of the TIF phenotype 72 h post-Cre.

Immunoblotting—Immunoblotting was performed as described previously (19). Briefly, cell extracts were made from MEFs using 450 mM NaCl lysis buffer (50 mM Tris-HCl (pH 7.4), 1% Triton X-100, 0.1% SDS, 450 mM NaCl, 1 mM EDTA, and 1 mM DTT) and protease inhibitors. Lysates were centrifuged at 13,200 rpm for 10 min. Protein concentrations from supernatants were determined using the Bradford protein assay (Bio-Rad). Samples were suspended in 2× sample buffer (75 mM Tris-HCl (pH 6.8), 10% glycerol, 2% SDS, 0.05% bromphenol blue, and 2.5% β-mercaptoethanol) prior to loading on 8 or 10% SDS-PAGE gels and then transferred to nitrocellulose membranes in transfer buffer (25 mM Tris, 0.192 M glycine, and 20% methanol). After blocking with 5% nonfat dry milk in PBST (PBS/0.1% Tween 20) at room temperature for 20 min, membranes were incubated in PBST for 1 h with the following primary antibodies: rabbit polyclonal anti-mTRF1 antibody (catalog no. 1449), rabbit polyclonal anti-mTRF2 antibody (catalog no. 1254), rabbit polyclonal anti-mRap1 antibody (catalog no. 1252), and mouse monoclonal anti-α-tubulin (Sigma-Aldrich); mouse monoclonal anti-MYC antibody (catalog no. 9E10, Calbiochem); and mouse monoclonal anti-HA antibody (catalog no. 12CA5, Roche). Membranes were developed with ECL (Amersham Biosciences).

Coimmunoprecipitation—Coimmunoprecipitations were performed as described previously (19). Cell extracts were made from MEFs or 293T cells using 150 mM NaCl lysis buffer (50 mM Tris-HCl (pH 7.4), 1% Triton X-100, 0.1% SDS, 150 mM NaCl, 1 mM EDTA, and 1 mM DTT) and protease inhibitors. Lysates were centrifuged at 13,200 rpm for 10 min. 1% of the supernatant was taken to serve as input. Following preclearing with protein G beads (GE Healthcare) for 30 min at 4 °C, supernatants were incubated with anti-HA affinity matrix (Roche) or anti-MYC affinity gel (catalog no. A7470, Sigma) overnight at 4 °C on a rotator wheel. Following three 10-min washes with lysis buffer, beads were pelleted by centrifugation and resuspended in 2× sample buffer (75 mM Tris-HCl (pH 6.8), 10% glycerol, 2% SDS, 0.05% bromphenol blue, and 2.5% β-mercaptoethanol) prior to loading on 8% or 10% SDS-PAGE gels and then transferred to nitrocellulose membranes in transfer buffer (25 mM Tris, 0.192 M glycine, and 20% methanol). Membranes were immunoblotted as described above.

Indirect Immunofluorescence—Cells were grown on coverslips and fixed with 2% paraformaldehyde in PBS for 10 min. Telomeric DNA FISH was combined with IF as described previously (8) using the following antibodies: polyclonal rabbit anti-TRF1 (catalog no. 644), polyclonal rabbit anti-mTRF2 (catalog no. 1254), polyclonal rabbit anti-mRap1 (catalog no. 1252), and polyclonal rabbit anti-human 53BP1 antibody (catalog no. NB 100-304, Novus); mouse monoclonal anti-MYC antibody (catalog no. 9E10, Sigma); and anti-HA antibody (catalog no. 12CA5, Roche). Secondary antibodies were Alexa Fluor 555 goat anti-rabbit IgG (Molecular Probes) or Rhodamine Red-X-conjugated donkey anti-mouse IgG (Jackson Immunoresearch

Laboratories). A FITC-TelC (FITC-OO-CCCTAACCCTAAC-CCTAA, Applied Biosystems) probe was used to detect telomeric DNA using the protocol developed in Ref. 21. DNA was stained with DAPI. Where noted, nucleoplasmic proteins were removed using Triton X-100 buffer (0.5% Triton X-100, 20 mM Hepes-KOH (pH 7.9), 50 mM NaCl, 3 mM $MgCl_2$, and 300 mM sucrose) on ice for 2 min prior to fixation with 2% paraformaldehyde in PBS. Digital images were captured with a Zeiss Axioplan II microscope with a Hamamatsu C4742-95 camera using Improvision OpenLab software.

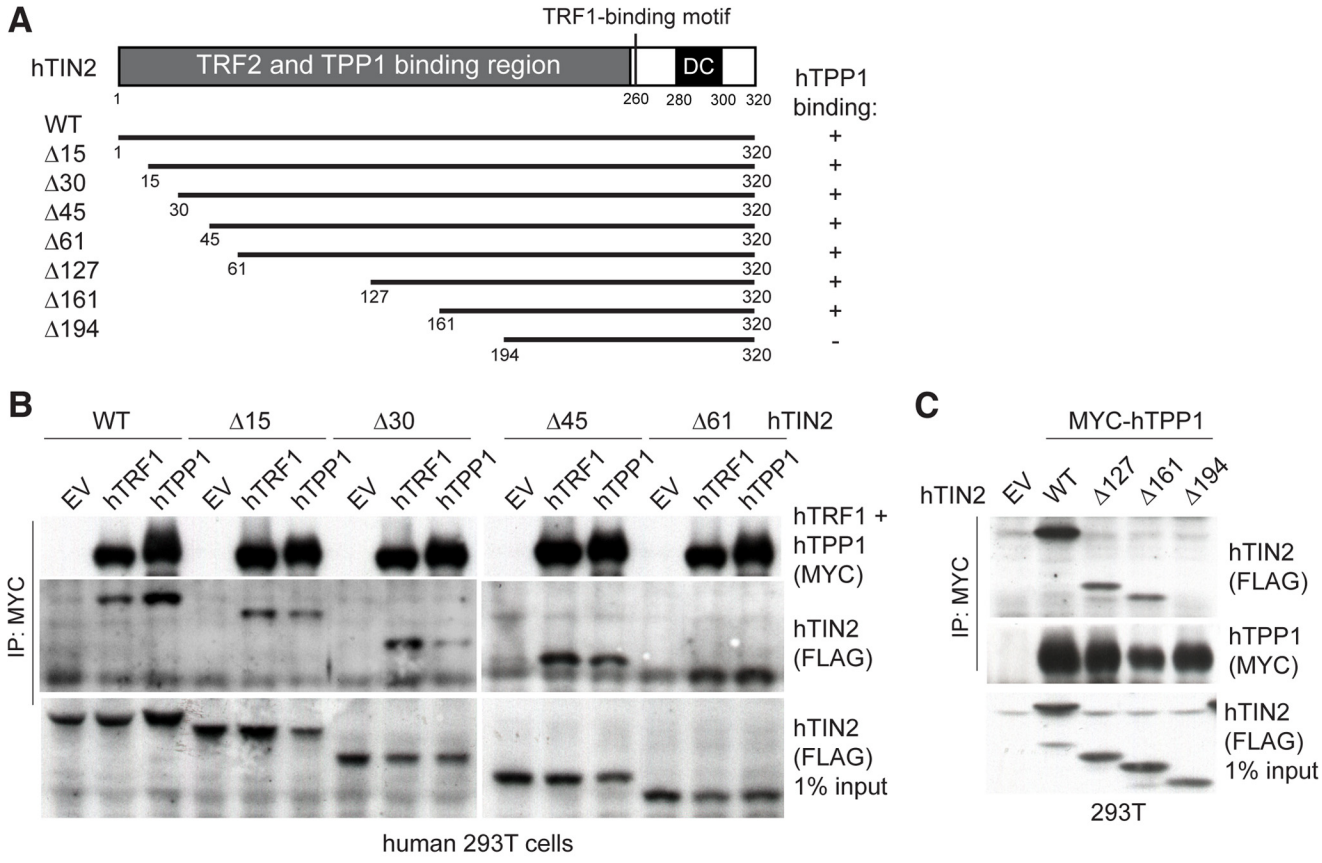

Chromatin Immunoprecipitation—ChIP was performed as described previously (22) with minor modifications. Cells were fixed in medium with 1% paraformaldehyde for 60 min at room temperature. Glycine was added to 0.2 M to stop the cross-linking. Cells were pelleted by centrifugation and washed once with cold PBS, followed by a final wash in PBS/1 mM PMSF. The cells were resuspended in cell lysis buffer (5 mM PIPES (pH 8.0), 85 mM KCl, 0.5% Nonidet P-40, 1 mM PMSF, and complete protease inhibitor mixture (Roche)) and incubated on ice for 15 min. After sonication, the lysates were centrifuged at 13,200 rpm for 10 min. The supernatants were incubated with commercial purified antibodies against MYC (catalog no. 9B11, Cell Signaling Technology) or HA (catalog no. 9110, Abcam). Samples were incubated at 4 °C overnight and for 45 min with ChIP-grade protein G magnetic beads (Dynal, Invitrogen). The immunoprecipitated DNA was collected and washed using a 16-tube magnetic separation rack (Cell Signaling Technology) and precipitated with ethanol after reversal of the cross-links. The DNA samples were dissolved in Tris-EDTA (TE), blotted using a slot blotter, and hybridized with an 800-bp probe labeled with Klenow and a primer for the C-rich telomeric repeat strand. The signal intensity measured by ImageQuant software was normalized to the signals of the input DNA on the same blot.

Telomere Analysis—Telomeric overhang signals and telomeric restriction fragment patterns were analyzed by in-gel analysis as described previously (9). Briefly, a [CCCTAA]4 oligonucleotide was hybridized to native MboI-digested genomic DNA fractionated on contour-clamped homogeneous electric field (CHEF) gels to determine the overhang signal. After capture of the signal, the DNA was denatured *in situ*, neutralized, and then rehybridized with the same probe to determine the total telomeric DNA signals. The overhang signal in each lane was normalized to the duplex telomeric signal so that comparisons of these ratios revealed changes in the overhang status. Signals originating from the wells were excluded from this quantification. The procedures for telomeric FISH on metaphase spreads were as described previously (23). Briefly, cells at the indicated time points and subjected to the indicated treatments were incubated for 2 h with 0.2 μg of colcemid/ml. The cells were harvested, swollen in 75 mM KCl, fixed in methanol/acetic acid (3:1), and dropped onto glass slides. After aging overnight, the slides were washed in 1× PBS for 5 min, followed by consecutive incubation with 75, 95, and 100% ethanol. The slides were allowed to air-dry before applying hybridizing solution (70% formamide, 1 mg/ml blocking reagent (Roche), and 10 mM Tris-HCl (pH 7.2)) containing a FITC-OO-[CCCTAA]3 peptide nucleic acid (PNA) probe (Applied Biosystems). The spreads were denatured for 3 min at 80 °C on a heat block and hybridized at room temperature for 2 h. The slides were washed twice for 15 min with 70% formamide/10 mM Tris-HCl (pH 7.0), followed by three 5-min washes in 0.1 M Tris-HCl (pH 7.0)/0.15 M NaCl/0.08% Tween 20. The chromosomal DNA was counterstained with DAPI added to the second wash. Slides were mounted in antifade reagent (ProLong Gold, Invitrogen), and digital images were captured with a Zeiss Axioplan II microscope with a Hamamatsu C4742-95 camera using Improvision OpenLab software.

RESULTS AND DISCUSSION

Generation of a TIN2 Allele That Does Not Bind TPP1—The N-terminal portion of human TIN2 from amino acids 1–257 is required to bind TRF2 and TPP1 (24). To define the human TIN2-TPP1 interaction site, a series of N-terminal hTIN2 truncation alleles (FLAG-tagged) were generated and assayed for human TPP1 binding in 293T cells (Fig. 1*A*). Coimmunoprecipitation analysis showed that MYC-tagged hTPP1 failed to interact with a truncated allele of hTIN2 that lacked amino acids 1–195, whereas deletion from 1–161 did not affect the interaction, pointing to sequences between 161 and 195 as the site of TPP1 interaction (Fig. 1, *B* and *C*). We next aimed to generate a mouse TIN2 allele that lacks the ability to bind to TPP1 because complementation of conditional TIN2 knockout MEFs have been proven previously to be an ideal setting for characterizing TIN2 binding mutants (19). After coimmunoprecipitation experiments, identification of conserved motifs, and analysis of predicted secondary structure (ExPASy), a mouse TIN2 allele lacking amino acids 132–188 (TIN2ΔTPP1) surrounding conserved predicted α-helices 7–9 was generated and introduced into previously characterized SV40-LT immortalized $TIN2^{F/F}$ MEFs (5). Coimmunoprecipitation analysis showed that mouse TIN2ΔTPP1 failed to bind exogenously expressed MYC-mTPP1, whereas this allele continued to interact normally with mTRF1 and mTRF2 (Fig. 1, *D*–*G*). Although deletion of TIN2 resulted in diminished TRF1 protein levels in TIN2-deleted cells, as observed previously (5), the protein levels of TRF1, TRF2, and Rap1 were unchanged in cells expressing TIN2ΔTPP1 (Fig. 2*H*).

Loss of TPP1 and POT1b from Telomeres in Cells Expressing TIN2ΔTPP1—As anticipated on the basis of the finding that TIN2 deletion compromises accumulation of TPP1 at telomeres (5), ChIP analysis for exogenous MYC-tagged TPP1 showed the loss of TPP1 at telomeres in cells expressing TIN2ΔTPP1 (Fig. 2, *A* and *B*). The level of TIN2ΔTPP1 at telomeres was similar to that of wild-type TIN2 (Fig. 2, *A* and *B*), consistent with previous findings that TIN2 requires only

FIGURE 1. **Generation of TIN2ΔTPP1.** *A*, schematic of shelterin binding in TIN2 and the FLAG-tagged N-terminal hTIN2 truncation alleles generated for binding studies. The TRF2 and TPP1 binding region identified previously is shown in *gray* (24). A *single line* demarcates TRF1 binding to TIN2 requiring Leu-260 (29), and the location of mutations identified in DC patients is shown in *black*. Human TPP1 binding capability is indicated. *B*, cell extracts from 293T cells coexpressing the indicated FLAG-tagged N-terminal hTIN2 truncation proteins, as shown in *A*, with MYC-hTPP1 or MYC-hTRF1 were immunoprecipitated (*IP*) with anti-MYC resin, and immunocomplexes were probed for the indicated proteins. *C*, cell extracts from 293T cells coexpressing the indicated FLAG-tagged hTIN2 truncation proteins, as shown in *A*, with MYC-hTPP1 were immunoprecipitated with anti-MYC resin, and immunocomplexes were probed for the indicated proteins. *D*, homology between human and mouse TIN2 and predicted secondary structure surrounding the TPP1-binding domain. Amino acids are shown in *red* and the *strikethrough* indicates a deletion introduced to generate TIN2ΔTPP1. *E*, schematic of mouse TIN2 indicating regions of TRF1, TRF2, and TPP1 binding and the corresponding location of mutations identified in DC patients. *F*, cell extracts from $TIN2^{F/F}$ MEFs exogenously expressing the indicated FLAG-HA2 mTIN2 alleles and MYC-mTPP1 were immunoprecipitated with anti-HA resin, and immunocomplexes were probed for the indicated proteins. *G*, cell extracts from 293T cells coexpressing the indicated FLAG-HA2 mTIN2 alleles and mTRF2 were immunoprecipitated with anti-HA resin, and immunocomplexes were probed with anti-HA and anti-mTRF2 antibodies. *H*, immunoblotting of cell extracts for the indicated proteins from $TIN2^{F/F}$ MEFs expressing mTIN2 alleles or EV with or without Cre treatment (72 h).

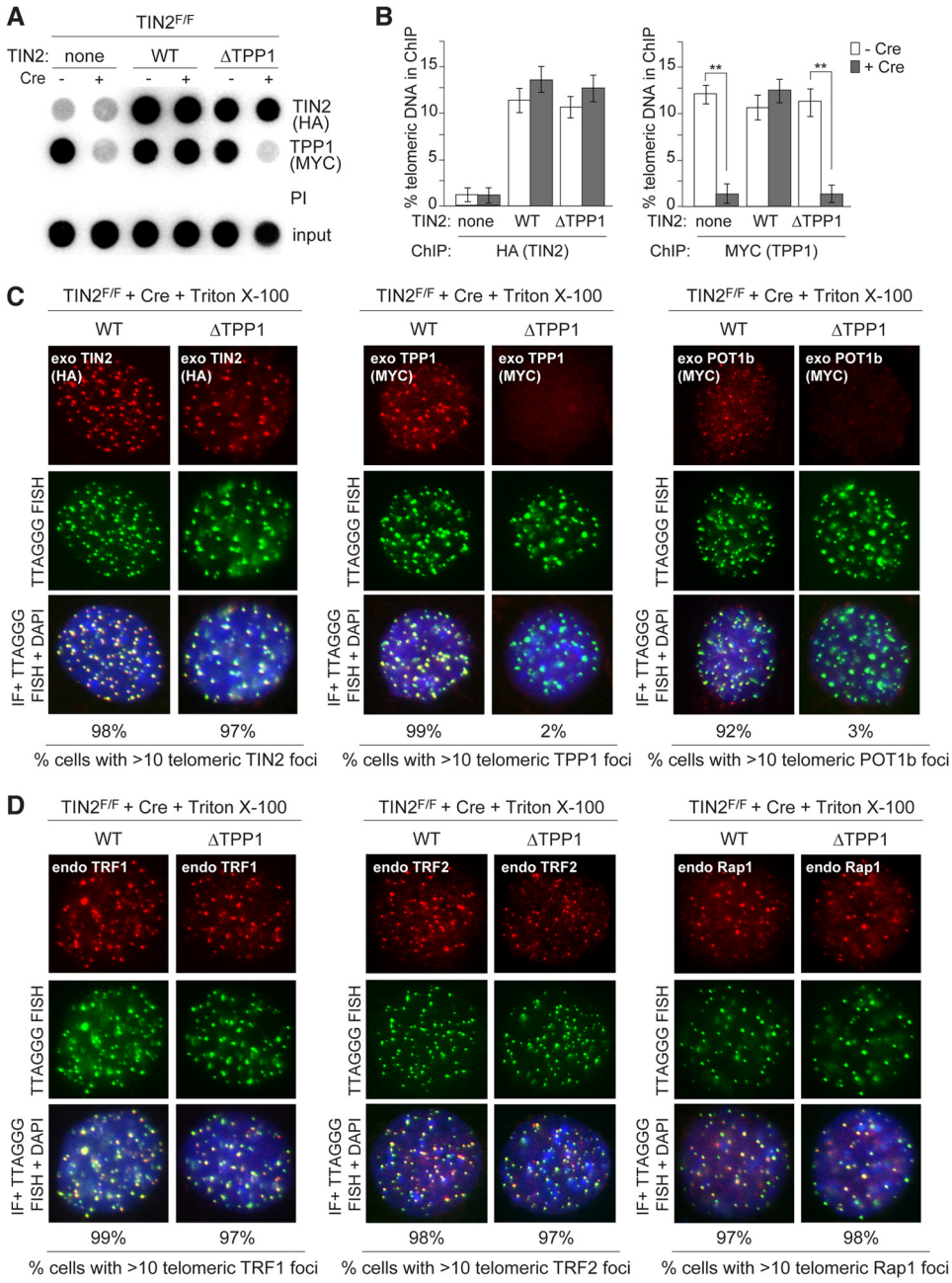

FIGURE 2. **TIN2 binding required for TPP1 and POT1b to localize to telomeres.** *A*, telomeric DNA ChIP for FLAG-HA2 TIN2 alleles (anti-HA) and MYC-TPP1 (anti-MYC) in TIN2$^{F/F}$ MEFs with or without Cre treatment (72 h). *PI*, preimmune. *B*, quantification of the ChIP signals from three identical experiments as in *A*. ChIP signals were normalized to the input, and the background (preimmune) was subtracted. *Error bars* represent mean ± S.D. **, $p < 0.05$ (paired Student's *t* test). *C*, indirect IF of FLAG-HA2 TIN2 alleles (anti-HA antibody, *red*, *left panel*), MYC-tagged TPP1 (anti-MYC antibody, *red*, *center panel*), or MYC-tagged POT1b (anti-MYC antibody, *red*, *right panel*) and telomeric FISH (*green*, *all panels*) following Triton X-100 extraction of soluble proteins in TIN2$^{F/F}$ MEFs (72 h post-Cre). DNA is stained with DAPI (*blue*). *exo*, exogenously expressed protein. *D*, IF of TRF1 (anti-TRF1 antibody, *red*, *left panel*), TRF2 (anti-TRF2 antibody, *red*, *center panel*), or Rap1 (anti-Rap1 antibody, *red*, *right panel*) and telomeric FISH (*green*, *all panels*) following Triton X-100 extraction of soluble proteins in TIN2$^{F/F}$ MEFs (72 h post-Cre). DNA was stained with DAPI (*blue*). *endo*, endogenously expressed protein.

TRF1 and TRF2 binding for optimal accumulation at telomeres (5, 19). Indirect IF and telomeric FISH further confirmed the proper localization of TIN2ΔTPP1 to telomeres, whereas MYC-tagged TPP1 (used instead of good antibodies for IF detection of endogenous TPP1) was correspondingly absent from telomeres when TIN2ΔTPP1 was the only TIN2 protein in the cells (Fig. 2*C*). Furthermore, consistent with the loss of POT1a and POT1b from telomeres following TIN2 or TPP1 deletion (5, 6), MYC-tagged POT1b (used instead of good IF antibodies for endogenous POT1b) was also undetectable via IF at telomeres in cells expressing TIN2ΔTPP1 (Fig. 2*C*). Localization of TRF1, TRF2, and Rap1 remained unperturbed in TIN2-deleted cells expressing the TIN2ΔTPP1 allele (Fig. 2*D*), which is expected because deletion of TPP1 does not appear to perturb the levels of TRF1, TRF2, or Rap1 at telomeres (6).

TIN2ΔTPP1 Leads to an ATR Kinase-dependent DNA Damage Response—Deletions of TIN2, TPP1, or POT1a and POT1b result in the activation of ATR-dependent DNA damage signal-

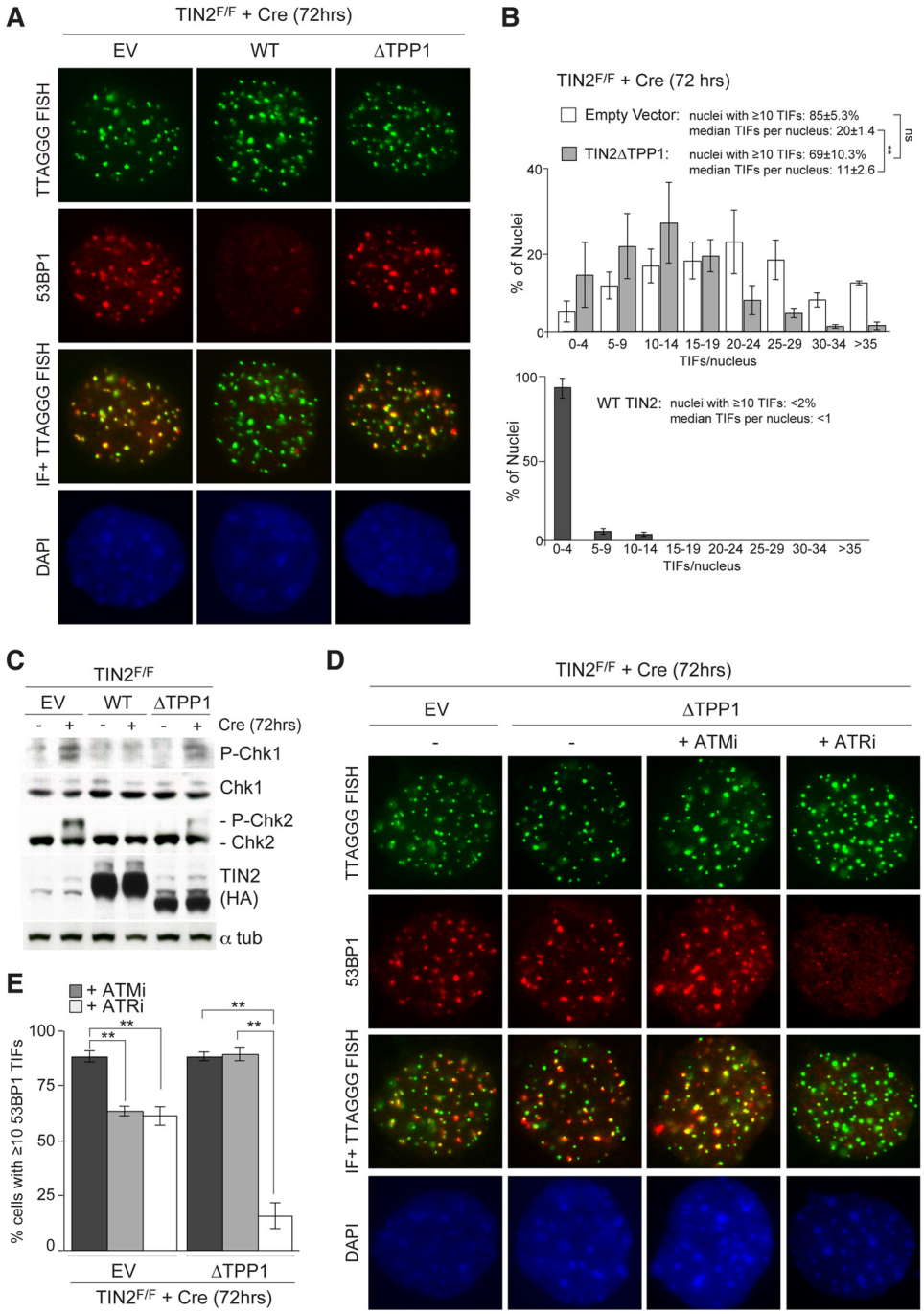

FIGURE 3. **DNA damage response in TIN2ΔTPP1-expressing cells is ATR-dependent.** *A*, IF of 53BP1 (*red*) and telomeric FISH (*green*) in TIN2$^{F/F}$ MEFs (72 h post-Cre) expressing an EV or the indicated FLAG-HA2 TIN2 alleles. DNA was stained with DAPI (*blue*). *B*, quantification of TIFs in TIN2$^{F/F}$ MEFs transduced with an empty vector or TIN2ΔTPP1 (shown together in the *top panel*) and wild-type TIN2 (*bottom panel*) as scored for 53BP1 TIFs per nucleus and TIF-positive nuclei (≥10 53BP1 foci at telomeres) ($n > 200$) after Cre (72 h). Data are mean ± S.D. from at least three independent experiments. **, $p < 0.05$ (paired Student's *t* test); *ns*, not significant. *C*, immunoblots for Chk1 and Chk2 phosphorylation in TIN2$^{F/F}$ MEFs expressing the indicated FLAG-HA2 TIN2 alleles and treated with Cre (72 h) as indicated. α-*tub*, α-tubulin. *D*, IF of 53BP1 (*red*) and telomeric FISH (*green*) in TIN2$^{F/F}$ MEFs (72 h post-Cre) expressing EV or TIN2ΔTPP1 with or without ATM inhibitor (*ATMi*) and ATRi. DNA was stained with DAPI (*blue*). *E*, quantification of TIF-positive nuclei (≥10 53BP1 foci at telomeres; $n \geq 200$) in TIN2$^{F/F}$ MEFs transduced with an EV or TIN2ΔTPP1 and treated with ATM inhibitor and ATRi after Cre (72 h) as in *D*. Data are mean ± S.D. from three independent experiments. **, $p < 0.05$ (paired Student's *t* test).

ing at telomeres and phosphorylation of Chk1 (5, 6, 8). Activation of Chk2 in TPP1 or POT1a,b-deficient cells can be observed at later time points (96 h post-Cre) and is likely due to the breakage of dicentric chromosomes that form from occasional telomere fusions (6, 8). Importantly, because TIN2 inherently contributes to TRF2-mediated repression of ATM, Chk2 phosphorylation is observed at much earlier time points following TIN2 deletion (72 h post-Cre) (5).

As detected on the basis of the presence of 53BP1-positive TIFs (25), the robust DNA damage response that follows TIN2 loss was repressed completely by expression of wild-type TIN2 but not by the TIN2ΔTPP1 allele (Fig. 3, *A* and *B*). However,

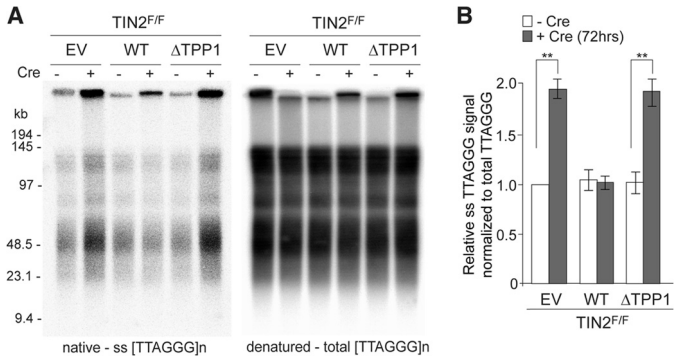

FIGURE 4. **Increase in single-stranded DNA accompanies loss of TPP1 binding to TIN2.** *A*, in-gel hybridization assay for single-stranded (*ss*) telomeric DNA after TIN2 deletion (72 h after Cre) in cells expressing EV, TIN2, or TIN2ΔTPP1. *Left panel*, TelC signals under native conditions. *Right panel*, the same gel rehybridized after *in situ* denaturation of the DNA. *B*, quantification of overhang signals from three independent experiments, as in *A*, normalized to the total telomeric signals and compared with TIN2$^{F/F}$ MEFs without Cre. **, $p < 0.05$ (paired Student's *t* test).

TIN2ΔTPP1-expressing cells had significantly fewer TIFs per nucleus compared with TIN2-deleted cells, suggesting that this allele is partially competent in repressing the DNA damage response (Fig. 3*B*). Chk1 phosphorylation was readily observed in TIN2-deleted cells expressing TIN2ΔTPP1 (72 h post-Cre), whereas wild-type TIN2 fully repressed this index of ATR signaling (Fig. 3*C*). Conversely, Chk2 phosphorylation was detectable at marginal levels in TIN2ΔTPP1-expressing cells 72 h post-Cre compared with a robust signal from samples transduced with the empty vector (EV) (Fig. 3*C*).

The contribution of the ATR and ATM kinases was determined using ATM and ATR inhibitors (ATM inhibitor or ATRi, respectively). As shown previously (5, 19), both ATM and ATR inhibition reduced the number of TIFs in TIN2-deleted cells. Conversely, only inhibition of the ATR kinase strongly reduced the telomere damage response in TIN2-deleted cells expressing TIN2ΔTPP1, whereas inhibition of the ATM kinase did not have a strong effect in this setting (Fig. 3, *D* and *E*). Together, these data suggest that TIN2ΔTPP1 expressed in TIN2-deficient cells results in the same ATR-dependent telomere damage phenotype as the loss of TPP1 and/or POT1a,b.

Excessive Single-stranded Telomeric DNA in the Absence of TPP1 Binding to TIN2—A characteristic phenotype associated with deletion of either TIN2, TPP1, or POT1b is an increase in the single-stranded TTAGGG repeats (5–7, 26–28). In-gel hybridization to quantify single-stranded telomeric DNA showed that this phenotype is recapitulated in TIN2$^{F/F}$ cells only expressing TIN2ΔTPP1 after introduction of Cre (72 h) (Fig. 4, *A* and *B*). The amount of single-stranded telomeric DNA increased ~2-fold in TIN2ΔTPP1-expressing cells, similar to cells infected with an empty vector control, whereas this change was not observed in the presence of wild-type TIN2 (Fig. 4, *A* and *B*). The increase in the single-stranded telomeric overhang observed in TIN2ΔTPP1 indicates that the binding of TPP1/POT1b to TIN2 is required for overhang maintenance.

TIN2ΔTPP1 Recapitulates the Pattern of Telomere Fusions Observed upon POT1a,b DKO—Expression of the TIN2ΔTPP1 allele did not improve the growth of TIN2$^{F/F}$ cells treated with

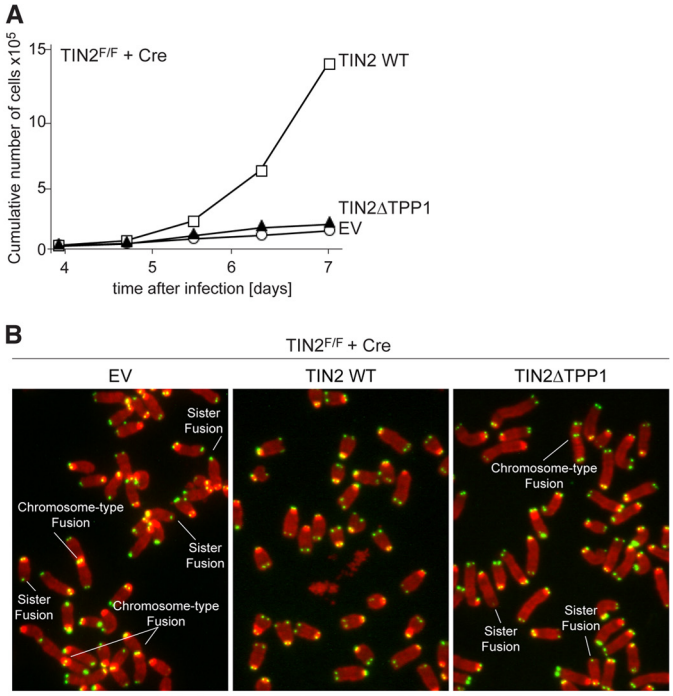

C

TIN2$^{F/F}$ + Cre	% of telomeres fused (avg.±SD) Chromosome-type		Chromatid-type		Sister (long arm)		% fragile telomeres
EV	13.7±2.1		2.1±0.40		7.3±0.64		2.6±0.64
TIN2 WT	<0.1	*a*	0	*b*	0	*c*	2.7±0.35
TIN2ΔTPP1	5.1±0.8		0.8±0.01		3.2±0.21		2.9±0.27

Values are from >2000 telomeres/experiment (n=3)
a, p<0.01; *b*, p=0.35; *c*, p<0.01

FIGURE 5. **TIN2ΔTPP1 recapitulates the POT1a,b DKO pattern of telomere fusions.** *A*, growth curve of SV40-LT-immortalized TIN2$^{F/F}$ MEFs expressing EV or the indicated FLAG-HA2 TIN2 alleles. *B*, examples of telomere fusions in metaphases of TIN2-deficient cells expressing the indicated TIN2 alleles or EV (72 h post-Cre). *Green*, TelC PNA probe; *red*, DAPI DNA stain. *C*, summary of telomere phenotypes in TIN2-deficient cells expressing TIN2 alleles, as determined by FISH and as shown in *B*. Data are mean ± S.D. from three independent experiments. Chromosome type, chromatid-type telomere, long-arm sister telomere fusions, and fragile telomeres were scored on 2000–3000 telomeres/experiment.

Cre (Fig. 5, *A*). Furthermore, TIN2ΔTPP1 was slightly defective in protecting telomeres from fusions, resulting in a low level of chromosome-type fusions after the introduction of Cre into TIN2$^{F/F}$ cells (Fig. 5, *B* and *C*). TIN2-deleted cells expressing TIN2ΔTPP1 also displayed a low frequency of sister telomere fusions (3%), whereas chromatid-type fusions involving telomeres from different chromosomes were almost never observed. The low frequency of these fusion events is comparable with the occasional telomere fusions (3–4%) reported after TPP1 or POT1a,b loss (6, 7). There were no statistically significant changes in the frequency of fragile telomeres observed between conditions, as expected, because TPP1/POT1a,b heterodimers do not appear to play a role in the DNA replication function of TRF1 (5). We conclude that each of the phenotypes associated with the loss of TPP1, POT1a, and POT1b are recapitulated faithfully by the TIN2ΔTPP1 allele.

CONCLUSIONS

The TPP1/POT1a and TPP1/POT1b heterodimers are critical for the protection of telomeres from ATR signaling and for

the maintenance of the correct structure at the telomere terminus. Using an allele of TIN2 that fails to bind TPP1 (TIN2ΔTPP1), we show that these heterodimers depend on their interaction with TIN2 to function correctly. Our results argue against the idea that POT1 proteins also have a functionally significant interaction with TRF2 (3, 11, 12) because the TIN2ΔTPP1 allele is fully competent in maintaining TRF2 at telomeres but fails to support the functions of POT1a and POT1b. Furthermore, the TIN2ΔTPP1 allele is fully capable of supporting the stabilization of TRF1 and TRF2/Rap1 at telomeres, arguing against a role for TPP1 in the assembly of the TIN2-TRF1-TRF2-Rap1 complex (12).

Acknowledgments—We thank the members of the de Lange laboratory for discussion of this work.

REFERENCES

1. Palm, W., and de Lange, T. (2008) How shelterin protects mammalian telomeres. *Annu. Rev. Genet.* **42,** 301–334
2. Xin, H., Liu, D., Wan, M., Safari, A., Kim, H., Sun, W., O'Connor, M. S., and Songyang, Z. (2007) TPP1 is a homologue of ciliate TEBP-β and interacts with POT1 to recruit telomerase. *Nature* **445,** 559–562
3. Barrientos, K. S., Kendellen, M. F., Freibaum, B. D., Armbruster, B. N., Etheridge, K. T., and Counter, C. M. (2008) Distinct functions of POT1 at telomeres. *Mol. Cell. Biol.* **28,** 5251–5264
4. Wan, M., Qin, J., Songyang, Z., and Liu, D. (2009) OB fold-containing protein 1 (OBFC1), a human homolog of yeast Stn1, associates with TPP1 and is implicated in telomere length regulation. *J. Biol. Chem.* **284,** 26725–26731
5. Takai, K. K., Kibe, T., Donigian, J. R., Frescas, D., and de Lange, T. (2011) Telomere protection by TPP1/POT1 requires tethering to TIN2. *Mol. Cell* **44,** 647–659
6. Kibe, T., Osawa, G. A., Keegan, C. E., and de Lange, T. (2010) Telomere protection by TPP1 is mediated by POT1a and POT1b. *Mol. Cell. Biol.* **30,** 1059–1066
7. Hockemeyer, D., Daniels, J. P., Takai, H., and de Lange, T. (2006) Recent expansion of the telomeric complex in rodents: two distinct POT1 proteins protect mouse telomeres. *Cell* **126,** 63–77
8. Denchi, E. L., and de Lange, T. (2007) Protection of telomeres through independent control of ATM and ATR by TRF2 and POT1. *Nature* **448,** 1068–1071
9. Celli, G. B., and de Lange, T. (2005) DNA processing is not required for ATM-mediated telomere damage response after TRF2 deletion. *Nat. Cell Biol.* **7,** 712–718
10. van Steensel, B., Smogorzewska, A., and de Lange, T. (1998) TRF2 protects human telomeres from end-to-end fusions. *Cell* **92,** 401–413
11. Chen, L. Y., Liu, D., and Songyang, Z. (2007) Telomere maintenance through spatial control of telomeric proteins. *Mol. Cell. Biol.* **27,** 5898–5909
12. O'Connor, M. S., Safari, A., Xin, H., Liu, D., and Songyang, Z. (2006) A critical role for TPP1 and TIN2 interaction in high-order telomeric complex assembly. *Proc. Natl. Acad. Sci. U.S.A.* **103,** 11874–11879
13. Nelson, N. D., and Bertuch, A. A. (2012) Dyskeratosis congenita as a disorder of telomere maintenance. *Mutat. Res.* **730,** 43–51
14. Savage, S. A., and Bertuch, A. A. (2010) The genetics and clinical manifestations of telomere biology disorders. *Genet. Med.* **12,** 753–764
15. Vulliamy, T., Beswick, R., Kirwan, M., Hossain, U., Walne, A., and Dokal, I. (2010) Telomere length measurement can distinguish pathogenic from non-pathogenic variants in the shelterin component, TIN2. *Clin. Genet.* **81,** 634–643
16. Sarper, N., Zengin, E., and Kılıç, S. Ç. (2010) A child with severe form of dyskeratosis congenita and TINF2 mutation of shelterin complex. *Pediatr. Blood Cancer* **55,** 1185–1186
17. Walne, A. J., Vulliamy, T., Beswick, R., Kirwan, M., and Dokal, I. (2008) TINF2 mutations result in very short telomeres: analysis of a large cohort of patients with dyskeratosis congenita and related bone marrow failure syndromes. *Blood* **112,** 3594–3600
18. Frescas, D., and de Lange, T. (2014) A TIN2 dyskeratosis congenita mutation causes telomerase-independent telomere shortening in mice. *Genes Dev.* **28,** 153–166
19. Frescas, D., and de Lange, T. (2014) TRF2-tethered TIN2 can mediate telomere protection by TPP1/POT1. *Mol. Cell. Biol.* **34,** 1349–1362
20. Toledo, L. I., Murga, M., Zur, R., Soria, R., Rodriguez, A., Martinez, S., Oyarzabal, J., Pastor, J., Bischoff, J. R., and Fernandez-Capetillo, O. (2011) A cell-based screen identifies ATR inhibitors with synthetic lethal properties for cancer-associated mutations. *Nat. Struct. Mol. Biol.* **18,** 721–727
21. Herbig, U., Jobling, W. A., Chen, B. P., Chen, D. J., and Sedivy, J. M. (2004) Telomere shortening triggers senescence of human cells through a pathway involving ATM, p53, and p21(CIP1), but not p16(INK4a). *Mol. Cell* **14,** 501–513
22. Loayza, D., and de Lange, T. (2003) POT1 as a terminal transducer of TRF1 telomere length control. *Nature* **423,** 1013–1018
23. Sfeir, A., Kabir, S., van Overbeek, M., Celli, G. B., and de Lange, T. (2010) Loss of Rap1 induces telomere recombination in the absence of NHEJ or a DNA damage signal. *Science* **327,** 1657–1661
24. Kim, S. H., Beausejour, C., Davalos, A. R., Kaminker, P., Heo, S. J., and Campisi, J. (2004) TIN2 mediates functions of TRF2 at human telomeres. *J. Biol. Chem.* **279,** 43799–43804
25. Takai, H., Smogorzewska, A., and de Lange, T. (2003) DNA damage foci at dysfunctional telomeres. *Curr. Biol.* **13,** 1549–1556
26. He, H., Wang, Y., Guo, X., Ramchandani, S., Ma, J., Shen, M. F., Garcia, D. A., Deng, Y., Multani, A. S., You, M. J., and Chang, S. (2009) Pot1b deletion and telomerase haploinsufficiency in mice initiate an ATR-dependent DNA damage response and elicit phenotypes resembling dyskeratosis congenita. *Mol. Cell. Biol.* **29,** 229–240
27. Hockemeyer, D., Palm, W., Wang, R. C., Couto, S. S., and de Lange, T. (2008) Engineered telomere degradation models dyskeratosis congenita. *Genes Dev.* **22,** 1773–1785
28. Wu, P., Takai, H., and de Lange, T. (2012) Telomeric 3′ overhangs derive from resection by Exo1 and Apollo and fill-in by POT1b-associated CST. *Cell* **150,** 39–52
29. Chen, Y., Yang, Y., van Overbeek, M., Donigian, J. R., Baciu, P., de Lange, T., and Lei, M. (2008) A shared docking motif in TRF1 and TRF2 used for differential recruitment of telomeric proteins. *Science* **319,** 1092–1096